











## RESEARCH ARTICLE

# Investigations of hypoxia-induced deoxyhemoglobin as a contrast agent for cerebral perfusion imaging

Ece Su Sayin<sup>1,2</sup>  | Jacob Schulman<sup>3,4</sup>  | Julien Poublanc<sup>5</sup>  |  
 Harrison T. Levine<sup>1,2</sup>  | Lakshmikumar Venkat Raghavan<sup>2</sup>  | Kamil Uludag<sup>4,5,6</sup>  |  
 James Duffin<sup>1,2</sup>  | Joseph A. Fisher<sup>1,2</sup>  | David J. Mikulis<sup>4,5</sup>  | Olivia Sobczyk<sup>2,5</sup> 

<sup>1</sup>Department of Physiology, University of Toronto, Toronto, Ontario, Canada

<sup>2</sup>Department of Anaesthesia and Pain Management, University Health Network, University of Toronto, Toronto, Ontario, Canada

<sup>3</sup>Department of Medical Biophysics, University of Toronto, Toronto, Ontario, Canada

<sup>4</sup>Techna Institute, University Health Network, Toronto, Canada

<sup>5</sup>Joint Department of Medical Imaging and the Functional Neuroimaging Lab, University Health Network, Toronto, Ontario, Canada

<sup>6</sup>Center for Neuroscience Imaging Research, Institute for Basic Science and Department of Biomedical Engineering, Sungkyunkwan University, Suwon, Republic of Korea

## Correspondence

Olivia Sobczyk, Department of Anaesthesia and Pain Management, University Health Network, University of Toronto, Toronto, ON, Canada.

Email: [olivia.sobczyk@uhn.ca](mailto:olivia.sobczyk@uhn.ca)

## Funding information

Holt-Hornsby and Andreae Vascular Dementia Research Unit in the Joint Department of Medical Imaging at the Toronto Western Hospital and the University Health Network; Institute for Basic Science, Suwon, Republic of Korea, Grant/Award Number: IBS-R015-D1

## Abstract

The assessment of resting perfusion measures (mean transit time, cerebral blood flow, and cerebral blood volume) with magnetic resonance imaging currently requires the presence of a susceptibility contrast agent such as gadolinium. Here, we present an initial comparison between perfusion measures obtained using hypoxia-induced deoxyhemoglobin and gadolinium in healthy study participants. We hypothesize that resting cerebral perfusion measures obtained using precise changes of deoxyhemoglobin concentration will generate images comparable to those obtained using a clinical standard, gadolinium. Eight healthy study participants were recruited (6F; age 23–60). The study was performed using a 3-Tesla scanner with an eight-channel head coil. The experimental protocol consisted of a high-resolution T1-weighted scan followed by two BOLD sequence scans in which each participant underwent a controlled bolus of transient pulmonary hypoxia, and subsequently received an intravenous bolus of gadolinium. The resting perfusion measures calculated using hypoxia-induced deoxyhemoglobin and gadolinium yielded maps that looked spatially comparable. There was no statistical difference between methods in the average voxel-wise measures of mean transit time, relative cerebral blood flow and relative cerebral blood volume, in the gray matter or white matter within each participant. We conclude that perfusion measures generated with hypoxia-induced deoxyhemoglobin are spatially and quantitatively comparable to those generated from a gadolinium injection in the same healthy participant.

## KEYWORDS

brain imaging, cerebral blood flow, cerebral blood volume, gadolinium, mean transit time, MRI, susceptibility contrast agents

## 1 | INTRODUCTION

Many common conditions such as smoking, high blood cholesterol, obesity, sedentary lifestyle, diabetes, hypertension, and aging result

in accumulating cerebrovascular pathologies, for example, small vessel disease (Hara et al., 2019), venous collagenosis (Gerald et al., 2017; Mutlu et al., 2018), chronic inflammation (Barbieri et al., 2003; Hardbower et al., 2013), and multiple subcortical infarcts

This is an open access article under the terms of the [Creative Commons Attribution-NonCommercial](https://creativecommons.org/licenses/by-nc/4.0/) License, which permits use, distribution and reproduction in any medium, provided the original work is properly cited and is not used for commercial purposes.

© 2022 The Authors. *Human Brain Mapping* published by Wiley Periodicals LLC.

(Norrving, 2008; White et al., 2013). The progression in cerebral vascular disease may remain subclinical initially, but can reach a threshold after which it manifests as progressive cognitive decline and sudden stroke (Heshmatollah et al., 2021). Early detection of disease progression would provide the opportunity for prophylactic and therapeutic interventions to modify the outcomes.

Vascular dysfunction may be identified by high resolution resting cerebral perfusion measures such as cerebral blood flow (CBF), mean transit time (MTT), and cerebral blood volume (CBV). These measures may enable detection and monitoring of the evolution of vascular lesions and their effects. However, such measures are infrequently performed due to high cost–benefit considerations (Elias Junior et al., 2008; Li et al., 2006; Rischpler et al., 2012). Magnetic resonance imaging (MRI) is a highly attractive imaging approach, but clinically accepted perfusion imaging sequences still require an intravascular injection of a gadolinium-based contrast agent (GBCA), which has sufficient pharmacological and clinical limitations to discourage its use for screening and monitoring for cerebrovascular disease. Drawbacks of GBCA include its invasiveness, expense (Nunn, 2006), leakage into the extracellular fluid (Quarles et al., 2019), accumulation in tissue (Kanda et al., 2014) and associated risks of causing harm (Gulani et al., 2017; Li et al., 2006; Runge, 2000). Noninvasive MRI alternatives to GBCA continue to be developed including arterial spin labeling which provides quantitative measures of CBF. However, this technique suffers from low spatial and temporal resolution (TR) and sensitivity to transit times which cause issues specifically for hemodynamic changes associated with widespread cerebrovascular dysfunction (Buxton et al., 1998; Mandell et al., 2008; van Gelderen et al., 2008).

Vu et al. (2021) have led the way in exploring the application of pulmonary hypoxia for increasing the concentration of dOHb ([dOHb]) in arterial blood for the purpose of providing susceptibility contrast in MRI. Poublanc et al. (2021) showed that one or two very brief (<60 s) episodes of pulmonary hypoxia-generate boluses of dOHb which are then propagated through the arterial system. The  $PO_2$  profile in the lungs is accurately reflected in the dOHb concentration versus time profile in the blood. The MRI signal changes in the brain enabled the calculation of resting cerebral perfusion measures consistent with those reported in the literature.

In this study, we compare the resting cerebral perfusion measures generated using hypoxia-induced dOHb with those calculated following the administration of a bolus of GBCA, in the same subject. We hypothesize that resting cerebral perfusion measures obtained using a precise hypoxia-induced dOHb concentration bolus will be comparable to those obtained using GBCA.

## 2 | METHODS

### 2.1 | Participants and ethics approval

This study conformed to the standards set by the latest revision of the Declaration of Helsinki and was approved by the Research Ethics

Board of University Health Network according to the guidelines of Health Canada. We recruited eight participants (6 M) between the ages of 23 and 60 ( $33.0 \pm 15.34$  years) by advertisement and word of mouth. All participants provided written and informed consent prior to scanning. All were healthy individuals, nonsmokers, not taking any medications, and with no history of neurological, cardiovascular or kidney diseases. All participant data were anonymized according to institutional protocols.

### 2.2 | Respiratory protocol

A computerized sequential gas delivery system, (RespirAct, Thornhill Medical, Toronto, Canada) was used to control end-tidal partial pressure of oxygen ( $P_{ET}O_2$ ) while maintaining normocapnia, independent of the pattern of participant ventilation (Fierstra et al., 2013; Fisher, 2016), where the  $P_{ET}CO_2$  and  $P_{ET}O_2$  are equivalent to the arterial partial pressures of  $CO_2$  ( $PaCO_2$ ) and  $O_2$  ( $PaO_2$ ) (Ito et al., 2008; Willie et al., 2012). Participants breathed through a face-mask sealed to the face with skin tape (Tegaderm, 3M, Saint Paul, MN) to exclude all but system-supplied gas. The programmed  $P_{ET}O_2$  stimulus pattern was 4 min and 20 s long (Figure 1). Arterial [dOHb] was calculated from  $P_{ET}O_2$  using the Hill equation describing the in vivo oxyhemoglobin dissociation curve (Balaban et al., 2013).

### 2.3 | MRI scanning protocol

A 3-Tesla scanner (HDx Signa platform, GE healthcare, Milwaukee, WI) with an eight-channel head coil was used in these experiments.

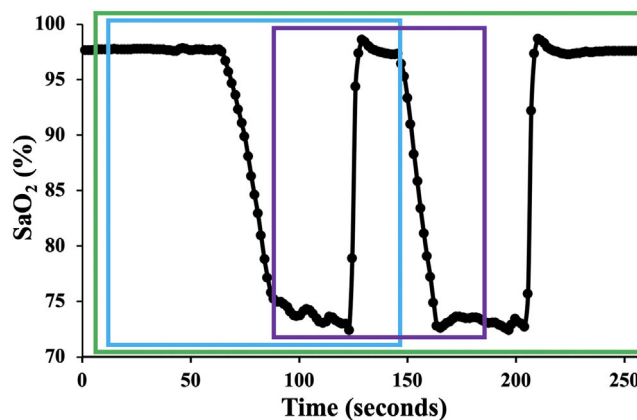


**FIGURE 1** The test protocol in a representative participant. The arterial  $O_2$  saturation ( $S_aO_2$ ) (black line) calculated from the  $P_{ET}O_2$  and the oxygen dissociation curve (Balaban et al., 2013). The protocol consisted of a 60 s baseline  $P_{ET}O_2$  of 95 mmHg (normoxia), a step decrease in  $P_{ET}O_2$  to 40 mmHg (hypoxia) for 60 s, a return to normoxia for 20 s, a step decrease in  $P_{ET}O_2$  to 40 mmHg for 60 s, followed by a return to normoxia for 60 s. The test protocol was divided into selected parts for separate analyses: “single hypoxic” step (blue rectangle), “double hypoxic” step (green rectangle), and “single normoxic” step with hypoxic baseline (purple rectangle)

The protocol consisted of a high-resolution T1-weighted scan followed by two BOLD sequence scans. The first BOLD scan sequence was acquired during  $P_{ET}O_2$  manipulation. A second scan was acquired at normoxia (room air breathing) following an intravenous injection of GBCA. For anatomical reference, a 3D T1-weighted inversion recovery fast-spoiled gradient-recalled sequence was used with the following parameters:  $T1 = 450$  ms,  $TR = 7.88$  ms,  $TE = 3$  ms, flip angle =  $12^\circ$ , voxel size =  $0.859 \times 0.859 \times 1$  mm, matrix size =  $256 \times 256$ , 146 slices, field of view =  $24 \times 24$  cm, no interslice gap. The BOLD data were acquired using a T2\*-weighted gradient echo echo planar imaging (EPI) sequence with the following parameters:  $TR = 1500$  ms,  $TE = 30$  ms, flip angle =  $73^\circ$ , 29 slices voxel size = 3 mm isotropic voxels and matrix size =  $64 \times 64$ . The number of EPI volumes acquired during the hypoxia-induced dOHb and GBCA protocols were 174 volumes and 47 volumes, respectively. After the completion of the  $P_{ET}O_2$  targeting protocol, the participant returned to free breathing of room air for at least 5 min before the GBCA perfusion acquisition for which 5 ml of Gadovist was injected intravenously at a rate of 5 ml/s (with a baseline delay of 30 s prior to injection) followed by 30 ml of saline at a rate of 5 ml/s.

## 2.4 | Data analysis basics

The acquired BOLD images were first volume registered, slice-time corrected and co-registered to their respective axial anatomical T1-weighted images using Analysis of Functional Neuroimaging (AFNI) software (National Institutes of Health, Bethesda, Maryland) (Cox, 1996). Analytical processing software (Statistical Parametric Mapping software (SPM8)) (Wellcome Department of Imaging Neuroscience, Institute of Neurology, University College, London, UK) (Ashburner & Friston, 2005) was then used to co-register each of the individuals T1-weighted images into Montreal Neurological Institute (MNI) standard space, as defined by a T1-weighted MNI152 standard template using a default 12-parameter affine transformation followed by nonlinear deformations (Ashburner & Friston, 1997). The calculated transformation for each participant was then applied to their respective BOLD images. Finally, the T1-weighted anatomical images in original space were segmented into cerebral spinal fluid, gray matter (GM), and white matter (WM) using SPM8 (Ashburner & Friston, 2005). The generated probability maps of GM and WM for each participant were thresholded at 70% probability and transformed into MNI space in the same manner as previously described. These maps permit the calculation of average GM and WM perfusion measures for GBCA and hypoxia-induced dOHb for comparison.

## 2.5 | Determining the BOLD signal change and the contrast to noise ratio

For each participant, the BOLD signal change ( $\Delta BOLD$ ) and contrast to noise ratio (CNR) were calculated for GBCA and for the selected parts of the hypoxia-induced dOHb protocol (Figure 1) for comparison.  $\Delta BOLD$  and CNR were calculated as follows: each voxel time

series was first divided by its own 20 s baseline mean and multiplied by 100 to scale the BOLD signal in percent. Then a linear regression of the BOLD signal against the whole brain average signal ( $\bar{S}$ , see below) as regressor was calculated and the slope determined the percent  $\Delta BOLD$ . The whole brain average signal ( $\bar{S}$ ) was used as the regressor to ensure both BOLD acquisitions could be compared. The regression calculation is summarized in Equation (1). Note that Equation (1) describes a multiple linear regression since a temporal signal drift component ( $\beta_1$ ) was added to the model.

$$S = \alpha \times \bar{S} + \beta_1 \times t + \beta_2 + \epsilon_t \quad (1)$$

where  $S$  is the scaled BOLD signal,  $\alpha$  is the slope of the regression (parameter of interest),  $\bar{S}$  is the one-dimensional time series regressor,  $\beta_1$  is the linear signal drift,  $\beta_2$  is the signal baseline, and  $\epsilon_t$  represents the residuals.

Using the slope of the regression ( $\alpha$ ),  $\Delta BOLD$  was calculated as follows:

$$\Delta BOLD = \alpha (\max(\bar{S}) - \min(\bar{S})) \quad (2)$$

where  $\max(\bar{S})$  and  $\min(\bar{S})$  are, respectively, the time points from the time series  $\bar{S}$  with maximum intensity and minimum intensity. Signal noise was determined as the standard deviation of the residuals from the linear regression,  $\text{std}(\epsilon_t)$ . To obtain CNR, the ratio of a signal difference ( $\Delta BOLD$ ) over the noise was calculated, as shown in Equation (3):

$$CNR = \frac{\Delta BOLD}{\text{std}(\epsilon_t)} \quad (3)$$

This method is described in greater detail in Poublanc et al. (2021). Average CNR and  $\Delta BOLD$  values for GM, WM, and GM/WM ratios were calculated for each participant.

## 2.6 | Calculating resting perfusion measures

Perfusion measures using hypoxia-induced dOHb were calculated using two different global arterial input functions (AIF): the BOLD signal measured over the middle cerebral artery (AIF-MCA) and the  $SaO_2$  (AIF- $SaO_2$ ) calculated from the  $P_{ET}O_2$ .  $SaO_2$  was resampled and interpolated to the TR interval (1500 ms) and time-aligned to the BOLD signal to match the rapid changes in  $SaO_2$  and BOLD signals. The BOLD signal measured over the MCA was also chosen as the AIF for the GBCA protocol. Signal smoothing in the temporal domain was applied voxel-wise to each data set using an adaptive mean filter with a width of seven time points.

VERBENA, FSL software (Chappell et al., 2015) was used to calculate MTT and relative CBF (rCBF) for the GBCA data and the data from the hypoxia-induced dOHb double hypoxic step protocol. In brief, VERBENA uses a Bayesian nonlinear model-fitting algorithm and a vascular model-based approach to treat the concentration of contrast agent in the tissue as the convolution of an identified AIF

and a residue function (Chappell et al., 2015). A series of parallel pathways of differing lengths are represented by a gamma distribution of transit times and converted to the equivalent residue function by integration. Once convolved with the residue function, the concentration time curve in the tissue can be calculated. This software also accounts for the susceptibility effects of nearby vessels.

Relative CBV (rCBV) was calculated as MTT multiplied by rCBF. Maps of the hypoxia-induced dOHb and GBCA perfusion measures were generated using AFNI software and overlaid onto their respective anatomical images. Within each participant, the ratio between average GM and WM for GBCA and the respective GM and WM averages for hypoxia-induced dOHb, were calculated in order to normalize them for comparison. Average values of GM and WM MTT, rCBF, and rCBV were calculated excluding obvious outliers likely generated by signal noise and partial volume effects (MTT from 0 to 10 s; rCBF from 0 to 0.1 a.u. and rCBV from 0 to 0.275 a.u.). The eliminated outliers constituted less than 6% of all voxels. Average resting perfusion measures for the eight participants were created by calculating voxelwise mean and SD of each perfusion measure, discussed in greater detail elsewhere (Sobczyk, 2015).

## 2.7 | Statistical analysis

Statistical comparisons within participants for CNR and  $\Delta$ BOLD values across all methods (GBCA and each selected section of the hypoxia-induced dOHb protocol) for GM, WM, and GM/WM ratios were performed using a two-way repeated measures analysis of variance (rmANOVA) with an all pairwise multiple comparisons correction using the Holm–Sidak method ( $\alpha = .05$ ). A two-way rmANOVA was performed on average MTT, rCBF, and rCBV values for GM and WM between GBCA (AIF-MCA), dOHb (AIF-MCA), and dOHb (AIF-SaO<sub>2</sub>) for each participant ( $\alpha = .05$ ).

## 3 | RESULTS

### 3.1 | The hypoxic stimulus

Induction of target hypoxia from normoxia was accomplished within 20 s in all participants. Reoxygenation within the sequence and at the

end of the sequence occurred within one to two breaths. The hypoxic periods were well tolerated by all participants. Only one of the participants reported transient moderate discomfort in the form of a sensation of shortness of breath.

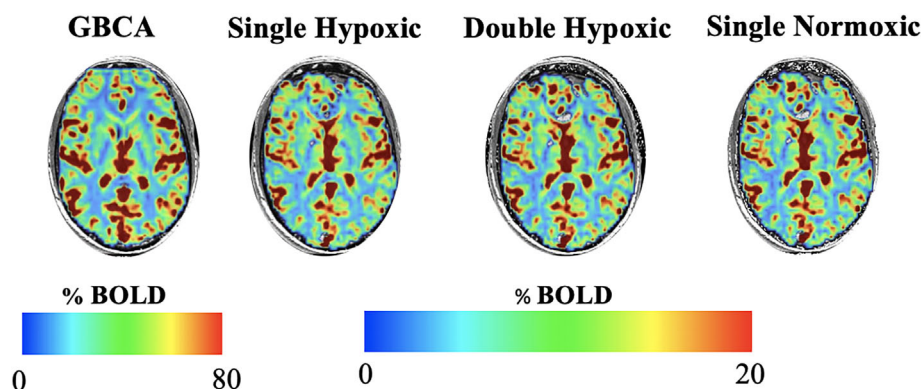
### 3.2 | The BOLD signal

The  $\Delta$ BOLD maps of a representative participant are shown in Figure 2 for GBCA and the three selected parts of the hypoxia-induced dOHb protocol consisting of single hypoxic, double hypoxic, and single normoxic portions. The average  $\Delta$ BOLD and CNR values for WM and GM are presented in Table 1.

$\Delta$ BOLD within the various parts of the hypoxic paradigm did not differ between subjects in GM or WM ( $p > .8$ ). However,  $\Delta$ BOLD was found to be significantly greater between GBCA and each of the hypoxia-induced dOHb paradigms in both GM and WM ( $p < .001$ ). The only significant difference in  $\Delta$ BOLD GM/WM ratio was found between GBCA and the single hypoxic part of the hypoxia-induced dOHb paradigm ( $p < .05$ ), which was significantly greater. GBCA CNR in GM was significantly greater than all hypoxic paradigms ( $p < .001$ ). There were no significant differences in CNR between hypoxic paradigms ( $p > .78$ ). Although all selected parts of the hypoxia-induced dOHb protocol yielded similar values, the double hypoxic sequence resulted in slightly higher  $\Delta$ BOLD and CNR (Table 1). Consequently, we chose the double hypoxic sequence of the hypoxia-induced dOHb protocol in the calculations of the perfusion measures for comparison with GBCA.

### 3.3 | Resting perfusion measures (MTT, rCBF, rCBV)

The perfusion measures, MTT, rCBF, and rCBV, were calculated for GBCA using an AIF from the MCA of each participant. Similarly, each measure was calculated for the hypoxia-induced dOHb double hypoxic paradigm using an AIF from the MCA and an AIF calculated from SaO<sub>2</sub> as indicated by the breath-by-breath P<sub>ET</sub>O<sub>2</sub>. Examples of each AIF waveform in a single participant are presented in Figure 3. The perfusion maps for a representative participant are shown in Figure 4. Resting cerebral perfusion maps for all participants may be found in the supplementary data (Figure S1).

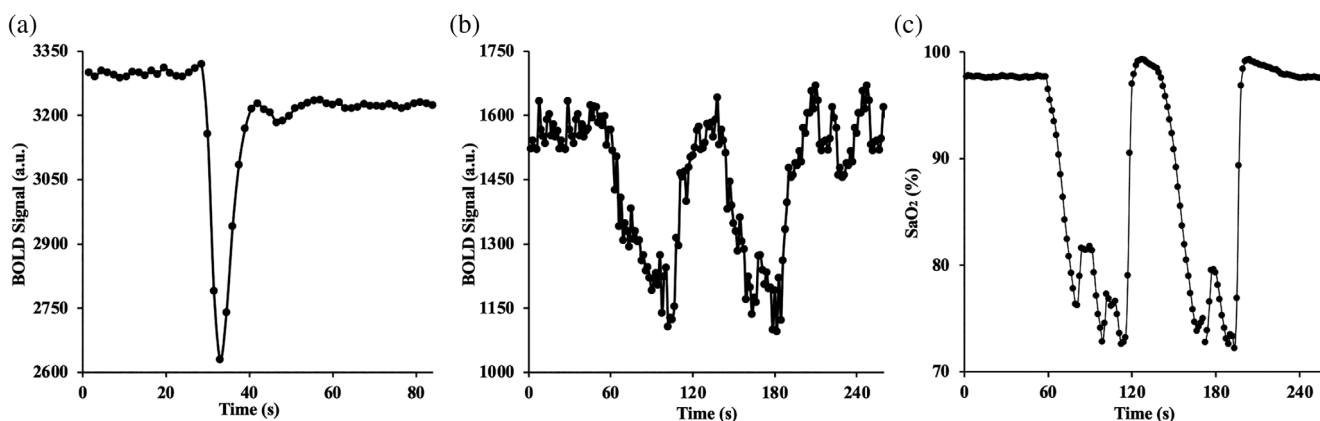


**FIGURE 2** The  $\Delta$ BOLD maps for a representative participant comparing selected paradigms of the protocol: single hypoxic, double hypoxic, and single normoxic to gadolinium (gadolinium-based contrast agent [GBCA]) contrast. Scaling the output range for the relative difference in signal strength enables the comparison of the deoxyhemoglobin measures to those of GBCA

**TABLE 1** Average (SD) measures of  $\Delta$ BOLD (%) and CNR calculated for GBCA, and the three selected parts of the protocol: single hypoxic, double hypoxic, and single normoxic changes for the eight participants

	$\Delta$ BOLD			CNR		
	GM (%)	WM (%)	GM/WM	GM	WM	GM/WM
GBCA	47.82 (11.26)	14.94 (3.68)	3.28	21.82 (4.42)	12.19 (2.86)	1.90
Single hypoxic	8.59 (4.09)	3.45 (1.64)	2.50	4.96 (1.34)	2.89 (0.97)	1.86
Double hypoxic	10.26 (3.63)	3.95 (1.50)	2.62	5.57 (1.52)	3.29 (0.91)	1.72
Single normoxic	9.19 (3.27)	3.70 (1.33)	2.51	4.92 (1.25)	3.09 (0.93)	1.64

Abbreviations: CNR, contrast to noise ratio; GBCA, gadolinium-based contrast agent; GM, gray matter; WM, white matter.

**FIGURE 3** The arterial input function (AIF) waveforms for a representative participant. (a) Gadolinium-based contrast agent (GBCA) arterial input function (AIF) BOLD signal (a.u.) versus time. (b) Hypoxia-induced dOHb AIF middle cerebral artery (MCA) BOLD signal (a.u.) versus time. (c) Hypoxia-induced dOHb AIF SaO<sub>2</sub> versus time

The collective averaged maps of the eight participants for the resting perfusion measures are shown in Figure 5. The average MTT, rCBF, and rCBV, in GM and WM for GBCA and the hypoxia-induced dOHb double hypoxic paradigm using both an AIF from the MCA and SaO<sub>2</sub> in the eight participants are displayed in Figure 6. A two-way repeated measures ANOVA comparison with an all pairwise multiple comparison procedure (Holm–Sidak method) found that MTT, rCBF, and rCBV measures using hypoxia-induced dOHb as a contrast agent were not significantly different between the three AIF waveforms in GM or WM ( $p < .05$ ) in any participant.

## 4 | DISCUSSION

### 4.1 | Main findings

The main finding of this exploratory study is that maps of resting perfusion measures using hypoxia-induced dOHb as a contrast agent displayed similar patterns and voxel-wise proportional changes in BOLD signal throughout the brain in all participants. The spatial distributions of each perfusion measure as generated by hypoxia-induced dOHb were consistent with those generated by the intravenous injection of GBCA (Figures 2 and 4). In addition, there were no statistically significant differences in MTT, rCBF, and rCBV in both GM and WM

between these contrast agents. All three hypoxia-induced dOHb paradigms showed comparable results with the double hypoxic paradigm having only a marginally higher  $\Delta$ BOLD and CNR (Table 1) suggesting that a simpler paradigm may prove to be suitable. Methodological, temporal, and individual participant variability was eliminated by using each participant as their own control. These findings indicate that resting cerebral perfusion measures obtained using specific patterns of precisely controlled hypoxia-induced changes in dOHb concentrations are comparable between subjects and to those obtained using GBCA.

### 4.2 | Methodological considerations

This study follows the recently published findings of Coloigner et al. (2020) and Vu et al. (2021), who demonstrated that abrupt increases in arterial [dOHb], induced by transient hypoxia, produce measurable changes in the BOLD MRI signal. Their reports noted the similarity of perfusion measures using dOHb as a contrast agent to past findings but did not directly compare their measures to those generated using GBCA.

Until recently, dOHb has not been considered for use as a susceptibility contrast agent due to the complicated nature of inducing the necessary precisely controlled changes in P<sub>ET</sub>O<sub>2</sub> in individuals. Vu

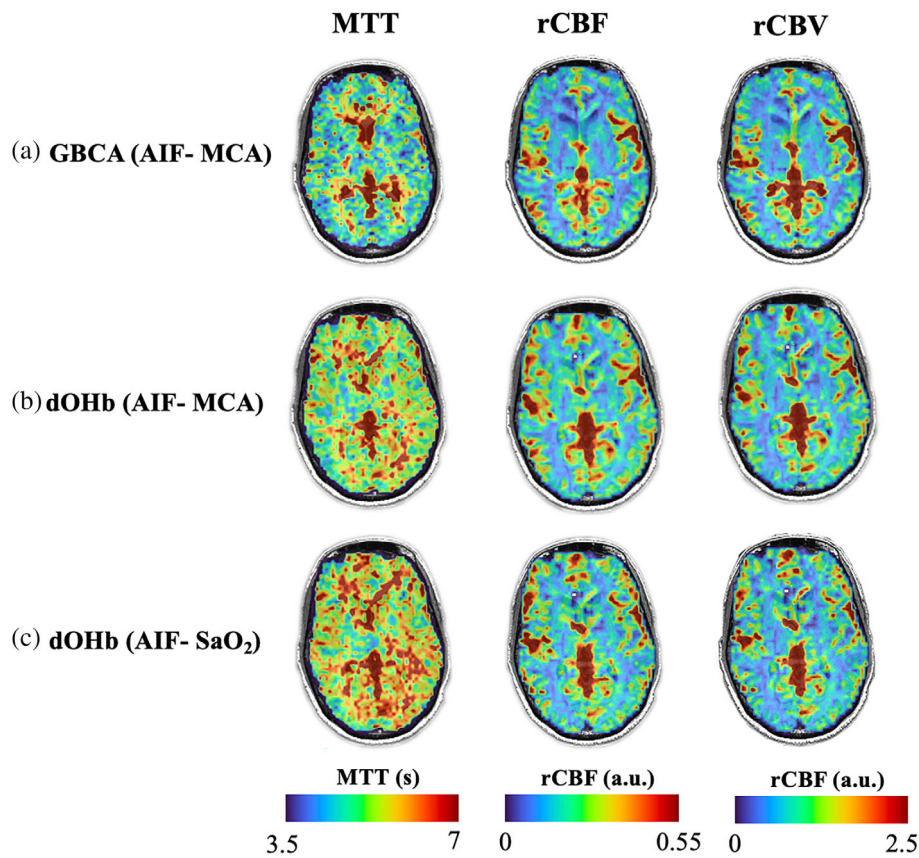


**FIGURE 4** Perfusion maps of mean transit time (MTT), relative cerebral blood flow (rCBF), and relative cerebral blood volume (rCBV) of a representative participant comparing the three arterial input functions (AIF) used to calculate them. (a) Gadolinium-based contrast agent (GBCA) (AIF middle cerebral artery [MCA]), (b) dOHb (AIF-MCA), and (c) dOHb (AIF-SaO<sub>2</sub>)

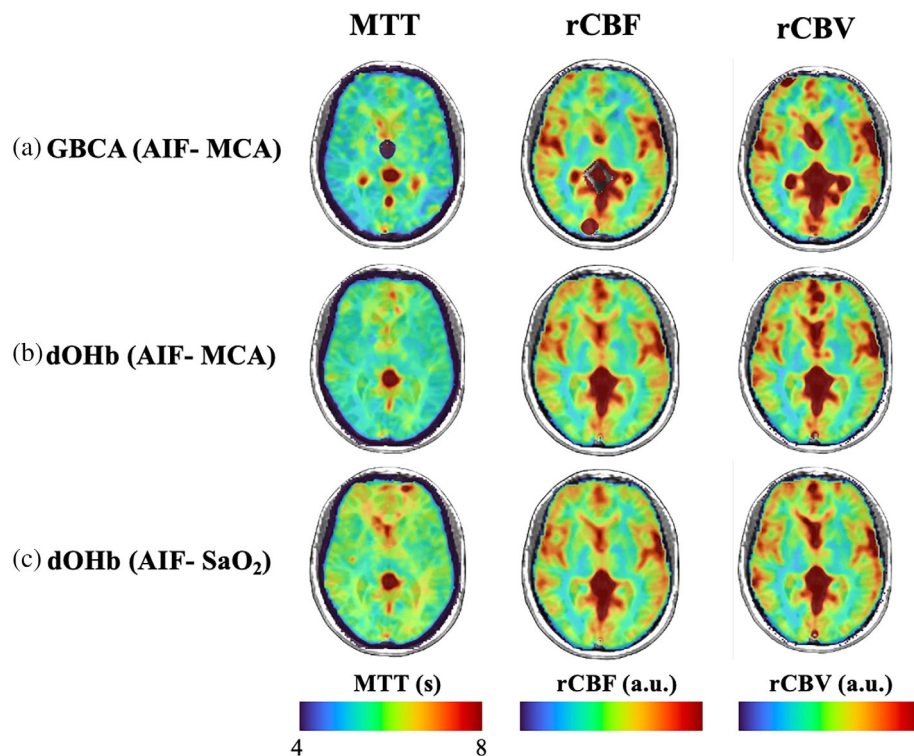


**FIGURE 5** Axial slice displaying the average resting perfusion measures (mean transit time [MTT], relative cerebral blood flow [rCBF], and relative cerebral blood volume [rCBV]) of the eight participants

et al. (2021) used inhaled nitrogen, a popular technique to produce a transient hypoxia (Pfoh et al., 2016), but without precise control. When using nitrogen as the source gas, and a 2 L reservoir on the

inspiratory limb to buffer the progress of hypoxia, the duration and magnitude of the reduction of  $P_{ET}O_2$  becomes highly sensitive to the subject's lung capacity and the pattern and extent of breathing

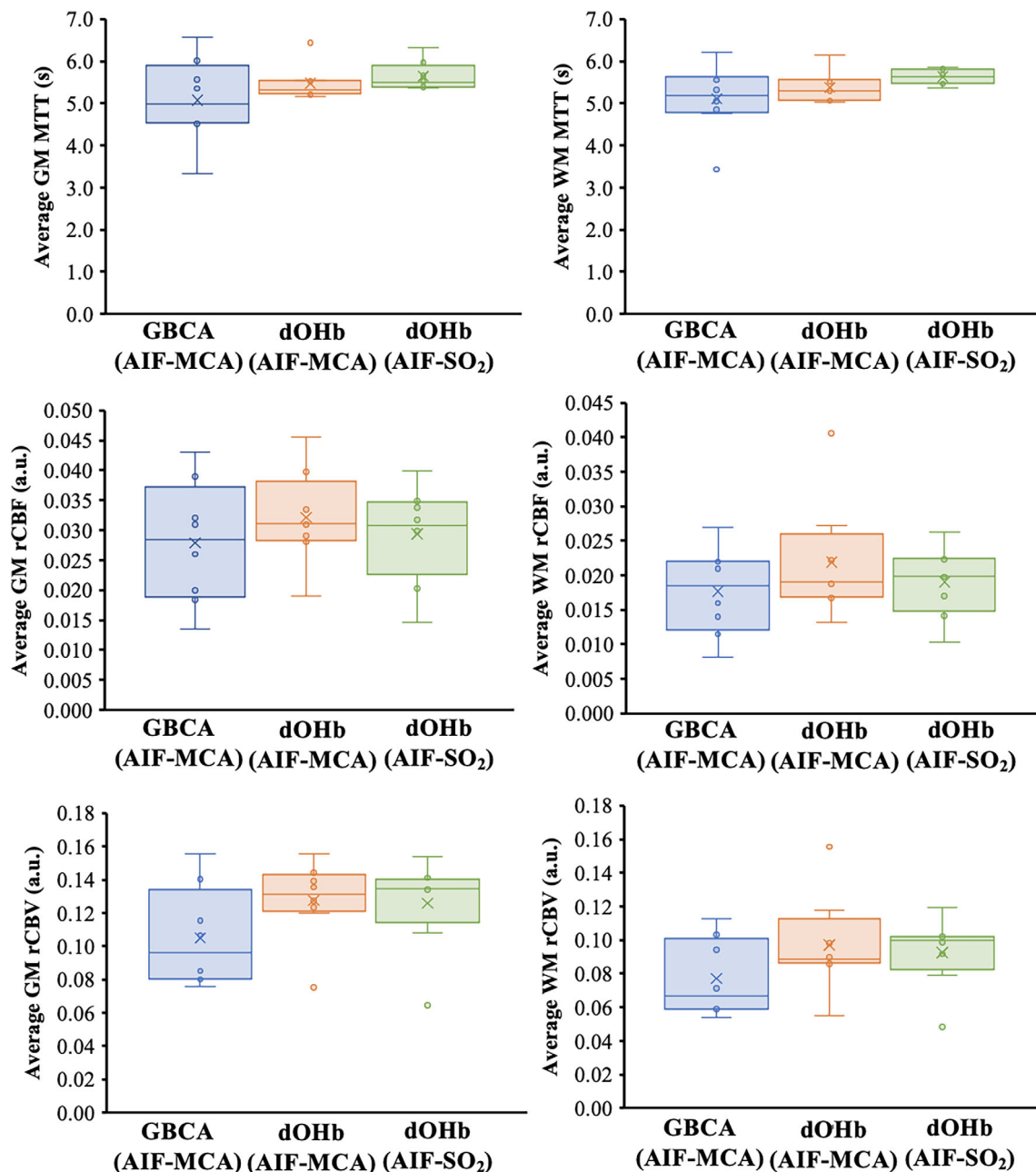


**FIGURE 6** Boxplots showing the distribution of mean transit time (MTT) (s), relative cerebral blood flow (rCBF) (a.u.), and relative cerebral blood volume (rCBV) (a.u.) measures for gadolinium-based contrast agent (GBCA), and the hypoxia-induced dOHb paradigms in gray matter (GM) and white matter (WM) for the eight participants. There is not a statistical significant difference after allowing for the effects of differences in WM/GM in any of the perfusion measures: MTT ( $p = .17$ ), rCBF ( $p = .21$ ), and rCBV ( $p = .151$ ). No significant differences were found in GM or WM for MTT, rCBF, and rCBV within each participant between the three arterial input function (AIF) waveforms ( $p > .05$ )

(Slessarev et al., 2007). Without precise control of the extent of hypoxia, there is a lack of consistency of the [dOHb] changes between subjects and between tests in the same subject.

In the current study, we used an automated gas delivery system (RespirAct, Thornhill Medical, Toronto, Canada). It uses a physiological model of the participant and sequential gas delivery (Fierstra et al., 2013; Slessarev et al., 2007) to prospectively provide the breath-by-breath inspired gas concentrations required to meet the target end-tidal gas partial pressures independently of the extent and

pattern of the participant's breathing. Although this automated system provided accurate target levels of hypoxia, the time course of transition from normoxia to hypoxia extended over about 20 s (Figure 1). This rate of change results from the kinetics of gas in the lungs which require the dilution of the gas in the functional residual capacity (i.e., the gas remaining in the lung after exhalation). By contrast, the resumption of normoxia can be achieved within one breath as there is a greater inspired gas to lung  $PO_2$  gradient available to raise lung  $PO_2$  (Fisher et al., 2016; Poublanc et al., 2021).

Previously, Poublanc et al. (2021) determined that CNR increased marginally with repeated hypoxic stimuli. In this study, we examined the CNR resulting from the three selected paradigms of the hypoxia-induced dOHb protocol and found little improvement between a single and double hypoxic bolus. Nevertheless, in this study, we used the data from the double hypoxic protocol as it had a slightly larger CNR (Table 1). CNR for hypoxia-induced dOHb is substantial, and further studies may yield a suitable compromise between a simpler protocol, lesser degree of hypoxia, and improved CNR.

For GBCA, abrupt changes in concentration are implemented by a rapid intravenous injection at 5 ml/s followed by a bolus of saline. Although the contrast is dispersed as it passes the right heart, loses contrast by leaking into the interstitium in the lungs, and mixes with the blood in the left heart, nevertheless, the MCA AIF achieves sufficiently rapid changes for analysis of perfusion measures (Figure 3). To achieve a sufficiently abrupt AIF from the hypoxia-induced dOHb paradigm it is necessary to implement an abrupt change of  $PO_2$  in the lung. However, abrupt changes are resisted by the dispersing effects of the inspired gases mixing with those remaining in the lungs after each previous expiration. Using the RespirAct, the concentration of inspired gases is precalculated to optimize the transition from existing, to target lung  $PO_2$  on the upcoming breath. In transitioning from lung normoxia to hypoxia, the washout of oxygen from the lung may take up to 20 s. However, reoxygenation of the lung and the reduction of deoxyhemoglobin in the arterial blood, can usually be accomplished in one or two breaths. Assuming a normal left ventricular ejection fraction, there will be little subsequent dispersion of this blood before arriving at the cerebral arteries. To the extent that the reoxygenation aspect of the hypoxia-induced dOHb paradigm approaches an ideal step change, it will contribute to the accuracy of the calculations of regional cerebral hemodynamics.

### 4.3 | Differences between GBCA and dOHb

As an intravascular paramagnetic molecule, dOHb has several characteristics that differ from those of GBCA (Supplementary Table 1). While GBCA distributes throughout the plasma, dOHb is confined to red blood cells. One consequence of this differing distribution is that [GBCA] increases as the hematocrit falls in the capillaries while [dOHb] increases (Calamante, 2010). Indeed, the intravascular [dOHb] can be known precisely (from its saturation and hematocrit) and therefore can be related to signal size whereas the [GBCA] is undeterminable. GBCA also passes readily out of capillaries into tissues such as the lungs resulting in dispersal before arrival in the cerebral arteries. In the brain, GBCA is contained intravascularly by the blood–brain barrier making it a good marker for its integrity, used, for example, in brain tumor investigations (Boxerman et al., 2006). By contrast, dOHb does not leak into tissues and remains intravascular regardless of the blood–brain barrier unless there is active bleeding. Finally, GBCA has seven unpaired electrons making it highly paramagnetic presenting the possibility of saturation of the BOLD signal inside blood vessels and interfering with the characterization of AIF and thereby any

resting perfusion measure calculations. Signal saturation is very unlikely to occur with hypoxia-induced dOHb which has only four unpaired electrons and a lesser magnetic moment.

### 4.4 | Hypoxia tolerance and safety

In designing this protocol, we estimated that a physiologically tolerable arterial  $PO_2$  of about 40 mmHg would produce an increase in [dOHb] of about 25% (Balaban et al., 2013) which would generate a scaled change in the BOLD signal to provide a perspective as to whether dOHb can be developed into a practical contrast agent. Previous studies performed in healthy subjects reported no distress at this level of hypoxia (Poublanc et al., 2021; Vu et al., 2021) and does not result in noticeable changes in respiratory rate and heart rate (Balaban et al., 2013; Battisti-Charbonney et al., 2011). Similar responses are reported for subjects with  $PO_2$  maintained at about 50 mmHg for longer than 20 min (Harris et al., 2013; Mahamed et al., 2003; Mahamed & Duffin, 2001) and at 55 mmHg for 8 h (Ren et al., 2001). Rebreathing tests at isoxic  $P_{ET}O_2$  of 40 and 50 mmHg are routinely employed for assessing respiratory chemoreflexes (Duffin, 2011) even in heart failure patients (Keir et al., 2020). Indeed, the exploration of the use of hypoxia-induced dOHb as a contrast agent is supported by the beneficial use of extended periods of intermittent hypoxia to benefit patients with myocardial infarction (Almendros et al., 2014; Nakada et al., 2017), heart failure (Serebrovskaya et al., 2008), hypertension (Ghofrani et al., 2006; Serebrovskaya et al., 2008), and cognitive decline (Navarrete-Opazo & Mitchell, 2014). Recently, Liu et al. (2020) in studies of intermittent hypoxia, reported that their elderly patients “safely tolerated cyclic, moderate hypoxemia which lowered  $SaO_2$  by 20–25%”. We know of no reports in the literature of ischemic crises or death induced by controlled brief transient hypoxia.

### 4.5 | Limitations

At this early stage, the use of [dOHb] as a susceptibility agent is far from optimized and conditions used in this study leave considerable room for further improvement. Further studies are required to determine the optimal hypoxia-induced dOHb protocol and the selected AIF for studies of people with healthy vasculature, as well as those with pathology. The scan sequence parameters also need to be optimized for whole brain coverage, TR and thereby CNR.

### 4.6 | Future directions

This study was a follow-up to previous work designed to provide some perspective of the hypoxia-induced dOHb approach by comparing it to a well-known clinical standard. We compared perfusion measures between hypoxia-induced dOHb and GBCA, but the considered gold standard for such measures uses positron emission tomography



(PET). Comparisons of GBCA and PET show only moderate consistency (Carroll et al., 2002; Grandin et al., 2005; Ostergaard et al., 1998). Nevertheless, it would be instructive to compare the maps of perfusion measures against this gold standard, particularly in patients with cerebrovascular disease. Larger studies are required to identify normal ranges of perfusion measures using hypoxia-induced dOHb as a contrast agent in population pools divided by age, sex, underlying diseases, and specific cerebrovascular pathophysiology.

## 5 | CONCLUSION

We conclude that using hypoxia-induced dOHb as a contrast agent provides a similar set of perfusion maps and measures to those using intravenously injected GBCA in the same healthy individuals. This finding supports the continued exploration of hypoxia-induced dOHb as a precisely controlled endogenous contrast agent which may prove to play a role in imaging resting perfusion measures in selected research and clinical studies.

### AUTHOR CONTRIBUTIONS

All authors contributed to the design and conceptualization of the study. Ece Su Sayin, Julien Poulblanc, James Duffin, and Olivia Sobczyk were involved in the data analysis. Ece Su Sayin, James Duffin, Joseph A. Fisher, and Olivia Sobczyk drafted the initial draft of the manuscript. All authors participated in multiple rounds of review of data and editing the manuscript. All authors have reviewed and endorsed the final draft.

### ACKNOWLEDGMENTS

All the authors thank Toronto Western Hospital MR technologist Keith Ta for all his help in acquiring the MR imaging data, Abby Skandaraniyam for study coordination and Dr. John Wood for feedback on the final draft of the paper. The study was supported by Holt-Hornsby and Andreae Vascular Dementia Research Unit in the Joint Department of Medical Imaging at the Toronto Western Hospital and the University Health Network. Kamil Uludag was supported by the Institute for Basic Science, Suwon, Republic of Korea (IBS-R015-D1).

### CONFLICT OF INTEREST

JAF and DJM contributed to the development of the automated end-tidal targeting device, RespirAct (Thornhill Research Inc., TRI) used in this study and have equity in the company. JAF, OS, and JD receive salary support from TRI. TRI provided no other support for the study. All other authors have no disclosures.

### DATA AVAILABILITY STATEMENT

Anonymized data will be shared by request from any qualified investigator for purposes such as replicating procedures and results presented in the article provided that data transfer is in agreement with the University Health Network and Health Canada legislation on the general data protection regulation.

### ORCID

Ece Su Sayin  <https://orcid.org/0000-0002-2419-751X>  
 Jacob Schulman  <https://orcid.org/0000-0002-9253-6499>  
 Julien Poulblanc  <https://orcid.org/0000-0001-8377-9846>  
 Harrison T. Levine  <https://orcid.org/0000-0002-6900-2659>  
 Lakshmi Kumar Venkat Raghavan  <https://orcid.org/0000-0002-1506-7000>  
 Kamil Uludag  <https://orcid.org/0000-0002-2813-5930>  
 James Duffin  <https://orcid.org/0000-0003-2270-7392>  
 Joseph A. Fisher  <https://orcid.org/0000-0001-8911-3543>  
 David J. Mikulis  <https://orcid.org/0000-0003-3956-0892>  
 Olivia Sobczyk  <https://orcid.org/0000-0001-8983-1043>

### REFERENCES

- Almendros, I., Wang, Y., & Gozal, D. (2014). The polymorphic and contradictory aspects of intermittent hypoxia. *American Journal of Physiology. Lung Cellular and Molecular Physiology*, 307(2), L129–L140. <https://doi.org/10.1152/ajplung.00089.2014>
- Ashburner, J., & Friston, K. (1997). Multimodal image coregistration and partitioning—A unified framework. *NeuroImage*, 6(3), 209–217.
- Ashburner, J., & Friston, K. J. (2005). Unified segmentation. *NeuroImage*, 26(3), 839–851. <https://doi.org/10.1016/j.neuroimage.2005.02.018>
- Balaban, D. Y., Duffin, J., Preiss, D., Mardimae, A., Vesely, A., Slessarev, M., Zubieta-Calleja, G. R., Greene, E. R., Macleod, D.B. & Fisher, J. A. (2013). The in-vivo oxyhaemoglobin dissociation curve at sea level and high altitude. *Respiratory Physiology & Neurobiology*, 186(1), 45–52. <https://doi.org/10.1016/j.resp.2012.12.011>
- Barbieri, M., Ferrucci, L., Corsi, A. M., Macchi, C., Lauretani, F., Bonafè, M., Olivieri, F., Giovagnetti, S., Franceschi, C. & Paolisso, G. (2003). Is chronic inflammation a determinant of blood pressure in the elderly? *American Journal of Hypertension*, 16(7), 537–543.
- Battisti-Charbonney, A., Fisher, J. A., & Duffin, J. (2011). Respiratory, cerebrovascular and cardiovascular responses to isocapnic hypoxia. *Respiratory Physiology & Neurobiology*, 179(2–3), 259–268.
- Boxerman, J. L., Schmainda, K. M., & Weisskoff, R. M. (2006). Relative cerebral blood volume maps corrected for contrast agent extravasation significantly correlate with glioma tumor grade, whereas uncorrected maps do not. *American Journal of Neuroradiology*, 27(4), 859–867.
- Buxton, R. B., Frank, L. R., Wong, E. C., Siewert, B., Warach, S., & Edelman, R. R. (1998). A general kinetic model for quantitative perfusion imaging with arterial spin labeling. *Magnetic Resonance in Medicine*, 40(3), 383–396. <https://doi.org/10.1002/mrm.1910400308>
- Calamante, F. (2010). Perfusion MRI using dynamic-susceptibility contrast MRI: Quantification issues in patient studies. *Topics in Magnetic Resonance Imaging*, 21(2), 75–85. <https://doi.org/10.1097/RMR.0b013e31821e53f5>
- Carroll, T. J., Teneggi, V., Jobin, M., Squassante, L., Treyer, V., Hany, T. F., Burger, C., Wang, L., Bye, A., Von Schulthess, G. K. & Buck, A. (2002). Absolute quantification of cerebral blood flow with magnetic resonance, reproducibility of the method, and comparison with H<sub>2</sub>(15)O positron emission tomography. *Journal of Cerebral Blood Flow and Metabolism*, 22(9), 1149–1156.
- Chappell, M. A., Mehndiratta, A., & Calamante, F. (2015). Correcting for large vessel contamination in dynamic susceptibility contrast perfusion MRI by extension to a physiological model of the vasculature. *Magnetic Resonance in Medicine*, 74(1), 280–290. <https://doi.org/10.1002/mrm.25390>
- Coloigner, J., Vu, C., Borzage, M., Bush, A., Choi, S., Miao, X., Chai, Y., Galarza, C., Lepore, N., Tamrazi, B., Coates, T. D. & Wood, J. C. (2020). Transient hypoxia model revealed cerebrovascular impairment

- in anemia using BOLD MRI and near-infrared spectroscopy. *Journal of Magnetic Resonance Imaging*, 52(5), 1400–1412. <https://doi.org/10.1002/jmri.27210>
- Cox, R. W. (1996). AFNI: Software for analysis and visualization of functional magnetic resonance neuroimages. *Computers and Biomedical Research*, 29(3), 162–173.
- Duffin, J. (2011). Measuring the respiratory chemoreflexes in humans. *Respiratory Physiology & Neurobiology*, 177(2), 71–79.
- Elias Junior, J., Santos, A. C. D., Koenigk-Santos, M., Nogueira-Barbosa, M. H., & Muglia, V. F. (2008). Complicações do uso intravenoso de agentes de contraste à base de gadolínio para ressonância magnética. *Radiologia Brasileira*, 41, 263–267.
- Fierstra, J., Sobczyk, O., Battisti-Charbonney, A., Mandell, D. M., Poublanc, J., Crawley, A. P., Mikulis, D. J., Duffin, J. & Fisher, J. A. (2013). Measuring cerebrovascular reactivity: What stimulus to use? *The Journal of Physiology*, 591(Pt 23), 5809–5821. <https://doi.org/10.1113/jphysiol.2013.259150>
- Fisher, J. A. (2016). The CO<sub>2</sub> stimulus for cerebrovascular reactivity: Fixing inspired concentrations vs. targeting end-tidal partial pressures. *Journal of Cerebral Blood Flow & Metabolism*, 36(6), 1004–1011. <https://doi.org/10.1177/0271678X16639326>
- Fisher, J. A., Iscoe, S., & Duffin, J. (2016). Sequential gas delivery provides precise control of alveolar gas exchange. *Respiratory Physiology & Neurobiology*, 225, 60–69. <https://doi.org/10.1016/j.resp.2016.01.004>
- Geraldes, R., Esiri, M. M., DeLuca, G. C., & Palace, J. (2017). Age-related small vessel disease: A potential contributor to neurodegeneration in multiple sclerosis. *Brain Pathology*, 27(6), 707–722.
- Ghofrani, H. A., Voswinkel, R., Reichenberger, F., Weissmann, N., Schermuly, R. T., Seeger, W., & Grimminger, F. (2006). Hypoxia- and non-hypoxia-related pulmonary hypertension – Established and new therapies. *Cardiovascular Research*, 72(1), 30–40. <https://doi.org/10.1016/j.cardiores.2006.07.025>
- Grandin, C. B., Bol, A., Smith, A. M., Michel, C., & Cosnard, G. (2005). Absolute CBF and CBV measurements by MRI bolus tracking before and after acetazolamide challenge: Repeatability and comparison with PET in humans. *NeuroImage*, 26(2), 525–535. <https://doi.org/10.1016/j.neuroimage.2005.02.028>
- Gulani, V., Calamante, F., Shellock, F. G., Kanal, E., Reeder, S. B., & International Society for Magnetic Resonance in Medicine. (2017). Gadolinium deposition in the brain: Summary of evidence and recommendations. *Lancet Neurology*, 16(7), 564–570. [https://doi.org/10.1016/S1474-4422\(17\)30158-8](https://doi.org/10.1016/S1474-4422(17)30158-8)
- Hara, M., Yakushiji, Y., Suzuyama, K., Nishihara, M., Eriguchi, M., Noguchi, T., Nishiyama, M., Nanri, Y., Tanaka, J. & Hara, H. (2019). Synergistic effect of hypertension and smoking on the total small vessel disease score in healthy individuals: The Kashima scan study. *Hypertension Research*, 42(11), 1738–1744. <https://doi.org/10.1038/s41440-019-0282-y>
- Hardbower, D. M., de Sablet, T., Chaturvedi, R., & Wilson, K. T. (2013). Chronic inflammation and oxidative stress: The smoking gun for *Helicobacter pylori*-induced gastric cancer? *Gut Microbes*, 4(6), 475–481.
- Harris, A. D., Murphy, K., Diaz, C. M., Saxena, N., Hall, J. E., Liu, T. T., & Wise, R. G. (2013). Cerebral blood flow response to acute hypoxic hypoxia. *NMR in Biomedicine*, 26(12), 1844–1852. <https://doi.org/10.1002/nbm.3026>
- Heshmatollah, A., Dommershuijsen, L. J., Fani, L., Koudstaal, P. J., Ikram, M. A., & Ikram, M. K. (2021). Long-term trajectories of decline in cognition and daily functioning before and after stroke. *Journal of Neurology, Neurosurgery and Psychiatry*, 92, 1158–1163. <https://doi.org/10.1136/jnnp-2021-326043>
- Ito, S., Mardimae, A., Han, J., Duffin, J., Wells, G., Fedorko, L., Minkovich, L., Katznelson, R., Meineri, M., Arenovich, T., Kessler, C. & Fisher, J. A. (2008). Non-invasive prospective targeting of arterial PCO<sub>2</sub> in subjects at rest. *The Journal of Physiology*, 586(15), 3675–3682.
- Kanda, T., Ishii, K., Kawaguchi, H., Kitajima, K., & Takenaka, D. (2014). High signal intensity in the dentate nucleus and globus pallidus on unenhanced T1-weighted MR images: Relationship with increasing cumulative dose of a gadolinium-based contrast material. *Radiology*, 270(3), 834–841. <https://doi.org/10.1148/radiol.13131669>
- Keir, D. A., Duffin, J., & Floras, J. S. (2020). Measuring peripheral chemoreflex hypersensitivity in heart failure. *Frontiers in Physiology*, 11, 595486. <https://doi.org/10.3389/fphys.2020.595486>
- Li, A., Wong, C. S., Wong, M. K., Lee, C. M., & Au Yeung, M. C. (2006). Acute adverse reactions to magnetic resonance contrast media gadolinium chelates. *British Journal of Radiology*, 79(941), 368–371. <https://doi.org/10.1259/bjr/88469693>
- Liu, X., Chen, X., Kline, G., Ross, S. E., Hall, J. R., Ding, Y., Mallet, R. T. & Shi, X. (2020). Reduced cerebrovascular and cardioventilatory responses to intermittent hypoxia in elderly. *Respiratory Physiology & Neurobiology*, 271, 103306. <https://doi.org/10.1016/j.resp.2019.103306>
- Mahamed, S., Cunningham, D. A., & Duffin, J. (2003). Changes in respiratory control after three hours of isocapnic hypoxia in humans. *Journal of Physiology (London)*, 547(1), 271–281.
- Mahamed, S., & Duffin, J. (2001). Repeated hypoxic exposures change respiratory chemoreflex control in humans. *The Journal of Physiology*, 534(Pt. 2), 595–603.
- Mandell, D. M., Han, J. S., Poublanc, J., Crawley, A. P., Kassner, A., Fisher, J. A., & Mikulis, D. J. (2008). Selective reduction of blood flow to white matter during hypercapnia corresponds with leukoaraiosis. *Stroke*, 39(7), 1993–1998.
- Mutlu, U., Swanson, S. A., Klaver, C. C. W., Hofman, A., Koudstaal, P. J., Ikram, M. A., & Ikram, M. K. (2018). The mediating role of the venules between smoking and ischemic stroke. *European Journal of Epidemiology*, 33(12), 1219–1228. <https://doi.org/10.1007/s10654-018-0436-2>
- Nunn, A. D. (2006). The cost of developing imaging agents for routine clinical use. *Investigative Radiology*, 41(3), 206–212.
- Nakada, Y., Canseco, D. C., Thet, S., Abdulsalam, S., Asaithamby, A., Santos, C. X., Shah, A. M., Zhang, H., Faber, J. E., Kinter, M. T., Szewda, L. I., Xing, C., Hu, Z., Deberardinis, R. J., Schiattarella, G., Hill, J. A., Oz, O., Lu, Z., ... Sadek, H. A. (2017). Hypoxia induces heart regeneration in adult mice. *Nature*, 541(7636), 222–227. <https://doi.org/10.1038/nature20173>
- Navarrete-Opazo, A., & Mitchell, G. S. (2014). Therapeutic potential of intermittent hypoxia: A matter of dose. *American Journal of Physiology. Regulatory, Integrative and Comparative Physiology*, 307(10), R1181–R1197. <https://doi.org/10.1152/ajpregu.00208.2014>
- Norrving, B. (2008). Leukoaraiosis and silent subcortical infarcts. *Revue Neurologique*, 164(10), 801–804. <https://doi.org/10.1016/j.neurol.2008.07.009>
- Ostergaard, L., Johannsen, P., Host-Poulsen, P., Vestergaard-Poulsen, P., Asboe, H., Gee, A. D., Hansen, S. B., Cold, G. E., Gjedde, A. & Gyldensted, C. (1998). Cerebral blood flow measurements by magnetic resonance imaging bolus tracking: Comparison with [(15)O]H<sub>2</sub>O positron emission tomography in humans. *Journal of Cerebral Blood Flow and Metabolism*, 18(9), 935–940. <https://doi.org/10.1097/00004647-199809000-00002>
- Pföh, J. R., Tymko, M. M., Abrosimova, M., Boulet, L. M., Foster, G. E., Bain, A. R., Ainslie, P. N., Steinback, C. D., Bruce, C. D. & Day, T. A. (2016). Comparing and characterizing transient and steady-state tests of the peripheral chemoreflex in humans. *Experimental Physiology*, 101(3), 432–447. <https://doi.org/10.1113/EP085498>
- Poublanc, J., Sobczyk, O., Shafi, R., Sayin, E. S., Schulman, J., Duffin, J., Ulludag, K., Wood, J. C., Vu, C., Dharmakumar, R., Fisher, J. A. & Mikulis, D. J. (2021). Perfusion MRI using endogenous deoxyhemoglobin as a contrast agent: Preliminary data. *Magnetic Resonance in Medicine*, 86(6), 3012–3021. <https://doi.org/10.1002/mrm.28974>
- Quarles, C. C., Bell, L. C., & Stokes, A. M. (2019). Imaging vascular and hemodynamic features of the brain using dynamic susceptibility contrast and dynamic contrast enhanced MRI. *NeuroImage*, 187, 32–55. <https://doi.org/10.1016/j.neuroimage.2018.04.069>

- Ren, X., Dorrington, K. L., & Robbins, P. A. (2001). Respiratory control in humans after 8 h of lowered arterial PO<sub>2</sub>, hemodilution, or carboxyhemoglobinemia. *Journal of Applied Physiology*, 90(4), 1189–1195.
- Rischpler, C., Park, M.-J., Fung, G. S. K., Javadi, M., Tsui, B. M. W., & Higuchi, T. (2012). Advances in PET myocardial perfusion imaging: F-18 labeled tracers. *Annals of Nuclear Medicine*, 26(1), 1–6. <https://doi.org/10.1007/s12149-011-0552-5>
- Runge, V. M. (2000). Safety of approved MR contrast media for intravenous injection. *Journal of Magnetic Resonance Imaging*, 12(2), 205–213. [https://doi.org/10.1002/1522-2586\(200008\)12:2<205::AID-JMRI1>3.0.CO;2-P](https://doi.org/10.1002/1522-2586(200008)12:2<205::AID-JMRI1>3.0.CO;2-P)
- Serebrovskaya, T. V., Manukhina, E. B., Smith, M. L., Downey, H. F., & Mallet, R. T. (2008). Intermittent hypoxia: Cause of or therapy for systemic hypertension? *Experimental Biology and Medicine*, 233(6), 627–650. <https://doi.org/10.3181/0710-MR-267>
- Slessarev, M., Han, J., Mardimae, A., Prisman, E., Preiss, D., Volgyesi, G., Ansel, C., Duffin, J. & Fisher, J. A. (2007). Prospective targeting and control of end-tidal CO<sub>2</sub> and O<sub>2</sub> concentrations. *The Journal of Physiology*, 581(3), 1207–1219.
- Sobczyk, O., Battisti-Charbonney, A., Poublanc, J., Crawley, A. P., Sam, K., Fierstra, J., Mandell, D. M., Mikulis, D. J., Duffin, J., & Fisher, J. A. (2015). Assessing cerebrovascular reactivity abnormality by comparison to a reference atlas. *Journal of Cerebral Blood Flow & Metabolism*, 35(2), 213–220. <https://doi.org/10.1038/jcbfm.2014.184>
- van Gelderen, P., de Zwart, J. A., & Duyn, J. H. (2008). Pitfalls of MRI measurement of white matter perfusion based on arterial spin labeling. *Magnetic Resonance in Medicine*, 59(4), 788–795. <https://doi.org/10.1002/mrm.21515>
- Vu, C., Chai, Y., Coloigner, J., Nederveen, A. J., Borzage, M., Bush, A., & Wood, J. C. (2021). Quantitative perfusion mapping with induced transient hypoxia using BOLD MRI. *Magnetic Resonance in Medicine*, 85(1), 168–181. <https://doi.org/10.1002/mrm.28422>
- White, C. L., Pergola, P. E., Szychowski, J. M., Talbert, R., Cervantes-Arriaga, A., Clark, H. D., Del Brutto, O. H., Godoy, I. E., Hill, M. D., Pellegrini, A., Sussman, C. R., Taylor, A. A., Valdivia, J., Anderson, D. C., Conwit, R., Benavente, O. R. & SPS3 Investigators. (2013). Blood pressure after recent stroke: Baseline findings from the secondary prevention of small subcortical strokes trial. *American Journal of Hypertension*, 26(9), 1114–1122. <https://doi.org/10.1093/ajh/hpt076>
- Willie, C. K., Macleod, D. B., Shaw, A. D., Smith, K. J., Tzeng, Y. C., Eves, N. D., Ikeda, K., Graham, J., Lewis, N. C., Day, T. A. & Ainslie, P. N. (2012). Regional brain blood flow in man during acute changes in arterial blood gases. *The Journal of Physiology*, 590(14), 3261–3275. <https://doi.org/10.1113/jphysiol.2012.228551>

#### SUPPORTING INFORMATION

Additional supporting information can be found online in the Supporting Information section at the end of this article.

**How to cite this article:** Sayin, E. S., Schulman, J., Poublanc, J., Levine, H. T., Raghavan, L. V., Uludag, K., Duffin, J., Fisher, J. A., Mikulis, D. J., & Sobczyk, O. (2023). Investigations of hypoxia-induced deoxyhemoglobin as a contrast agent for cerebral perfusion imaging. *Human Brain Mapping*, 44(3), 1019–1029. <https://doi.org/10.1002/hbm.26131>